SIMULATING GNSS-R DELAY-DOPPLER MAP OF OIL SLICKED SEA SURFACES UNDER GENERAL SCENARIOS

Chen Li and Weimin Huang[*]

Faculty of Engineering and Applied Science, Memorial University, St. John's, NL A1B 3X5, Canada

Abstract—Presently, the simulated Delay Doppler Maps (DDMs) of oil slicked sea are limited to simplified scenarios which have the elevation angle of 90° (nadir reflection). In this paper, the detailed simulation process to generate GNSS-R DDMs of oil slicked sea surfaces under general scenarios is presented. The DDM of oil slicked sea surface under general scenarios are generated by combining the mean-square slope model for oil slicked/clean surfaces and the GNSS-R Zavorotny-Voronovich (Z-V) scattering model. The coordinate system transformation appropriate for general-elevation-angle scenarios are also incorporated. To validate the proposed approach, a comparison is made between the DDMs of a simplified scenario and a general scenario, which are generated based on the oil slick distribution of the Deepwater Horizon oil spill accident. Theoretical analysis reveals that oil slick may be detected within a 100 km radius coverage area around the specular point for a GNSS-R receiver under the general scenario with elevation angles of 72°.

1. INTRODUCTION

During the past 20 years, navigation satellite system reflectometry (GNSS-R) has shown a great potential in remote sensing over ocean, land and ice [1–5]. Significant efforts have been put into retrieving the ocean surface parameters such as wind speed, mean sea level and significant wave height. Analysis of oil spills on sea surface with coastal radar was documented in [6]. Recently the possibility of detecting oil slicks using GNSS-R has been investigated [7]. It is based on scattering coefficient retrieval using DDMs. However, the DDM proposed in [7]
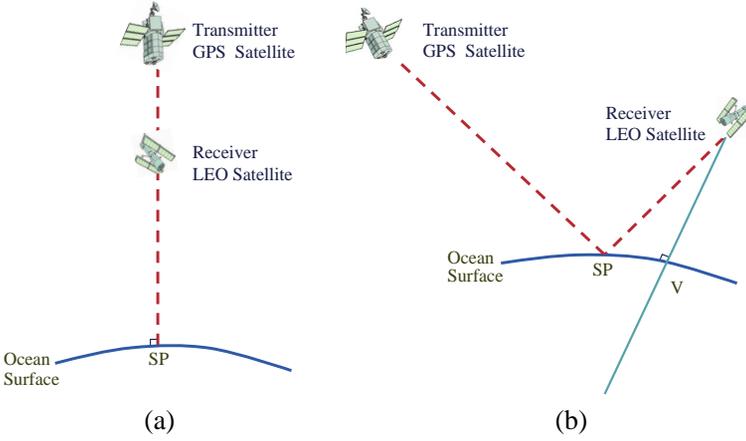
Figure 1. (a) Simplified scenario with the elevation angle of 90°. (b) General scenario.

is generated in a simplified scenario in which the elevation angle of the scenario is 90° (nadir reflection) as shown in Fig. 1(a). As this simplified scenario rarely exists, this paper proposes the detailed process of generating simulated DDMs of oil slicked areas that can be used in more general scenarios as shown in Fig. 1(b).

The proposed DDM simulating process of oil slicked areas is based on the combination of the oil-slicked sea surface scattering model [7] and the scattering model in the software receiver of Gleason [8]. Particularly, [7] incorporate the oil spill distribution in DDMs while [8] provides the routine of GNSS-R DDM generation under general scenarios.

This paper is organized as follows. Section 2 briefly introduces the theory of DDM simulation. Section 3 describes the glistening zone determination and mapping power distribution from spatial domain to the DD domain. In Section 4, the simulation results under the simplified scenario and general scenario are compared and discussed. Finally, Section 5 summarizes the main conclusions of this paper.

2. BASIC THEORY OF DDM SIMULATION

Delay Doppler Maps depict the power distribution of the signals scattered from the glistening zone in the DD domain. It can be expressed as [9]

$$\langle |Y(\Delta\tau, \Delta f)|^2 \rangle = T_i^2 \iint_A \frac{D^2(\vec{\rho})\sigma^0(\vec{\rho})\Lambda^2(\Delta\tau)|S(\Delta f)|^2}{4\pi R_R^2(\vec{\rho})R_T^2(\vec{\rho})} d^2\rho \quad (1)$$

where

|	
σ^0	scattering coefficient;
$\vec{\rho}$	position vector of a surface point relative to specular point;
D	antenna radiation pattern;
R_R	distance from the GNSS-R receiver to a point on the ocean surface;
R_T	distance from the transmitting satellite to a point on the ocean surface;
T_i	coherent integration time;
A	glistening zone;
$\langle |Y(\Delta\tau, \Delta f)|^2 \rangle$	power expression of received signal;
$\Delta\tau = \tau(\vec{\rho}) - \tau$	τ and $\tau(\vec{\rho})$ are the C/A delay of specular point and the observed surface point, respectively;
$\Delta f = f_d(\vec{\rho}) - f_d$	f_d and $f_d(\vec{\rho})$ are the Doppler frequency of the specular point and the observed surface point, respectively.
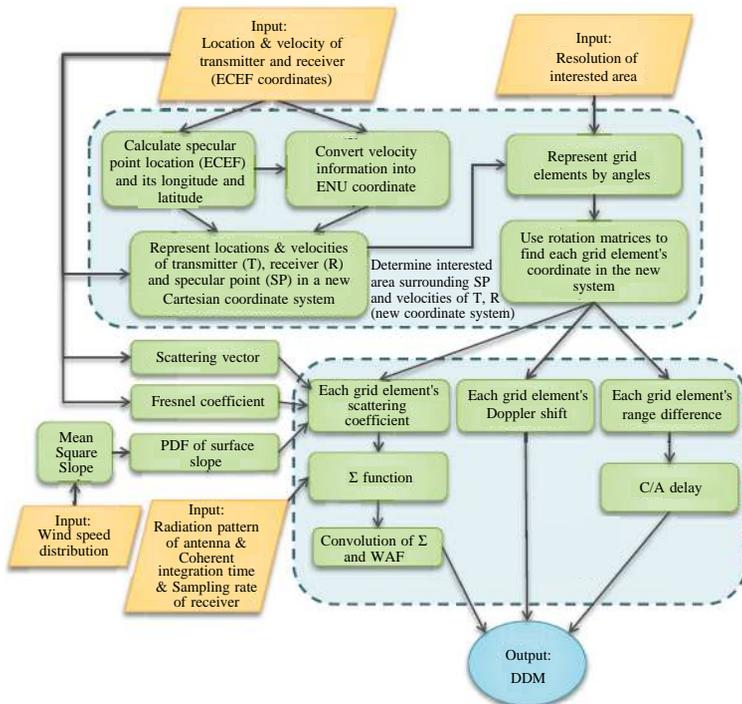
Figure 2. Flow chart of DDM simulation.

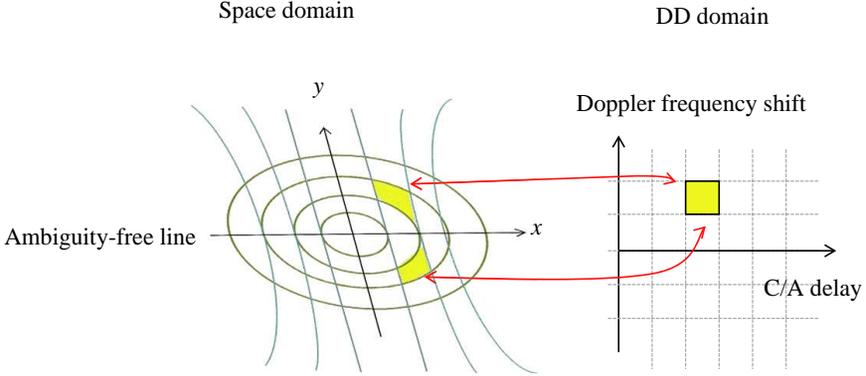Space domain   DD domain

Figure 3. Relationship between spatial domain and the DD domain. The blue lines indicate iso-Doppler; the purple lines indicate iso-range and the patches indicate grid elements.

The triangle function is defined as $\Lambda(\Delta\tau) = 1 - |\Delta\tau|/\tau_c$ if $|\Delta\tau| < \tau_c$, and $\Lambda(\Delta\tau) = 0$ elsewhere. $\tau_c = 1\,\text{ms}/1023$ is the length of a chip of the C/A code. The function $S(\Delta f)$ is defined as $S(\Delta f) = \sin(\pi T_i \Delta f)/(\pi T_i \Delta f)$. The observed area A is approximately the glistening zone, which is determined by the area that scatters enough power to be detected by the GNSS-R receiver.

As can be seen in Eq. (1), in order to generate a DDM, the location and scope of A needs to be determined first. Secondly, since grid elements (defined in Fig. 3) are on the spherical surface of the earth, an accurate way is required to obtain their coordinates. The third step is to determine the relationship between spatial domain $\vec{\rho}$ and the DD domain $(\Delta\tau, \Delta f)$. Finally, the simulation of DDM could be conducted using Eq. (1). A more detailed process can be seen in the flow chart in Fig. 2.

3. DETAILED METHODOLOGY OF DDM SIMULATION

This section explains the detailed DDM simulation process which includes three steps: 1) determine the location of the glistening zone surrounding the Specular Point (SP) in the Earth-Centered, Earth-Fixed (ECEF) coordinate System [10]. 2) obtain the coordinates of the grid elements in this glistening zone. 3) map the power scattered from glistening zone into the DD domain. The first two steps are the main process of extending the simplified scenario to a general scenario.
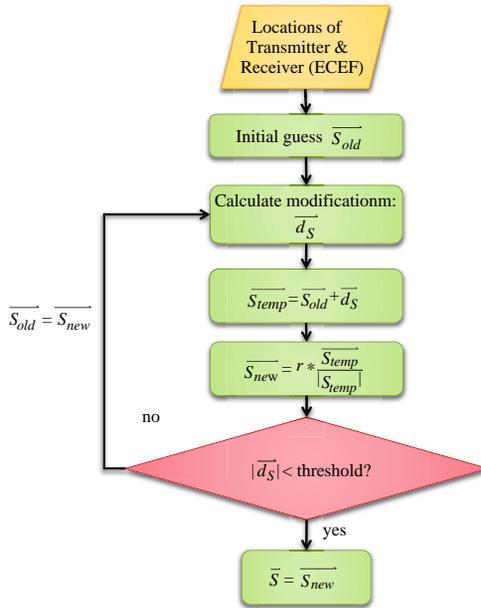
Figure 4. Flow chart of determining SP.

3.1. Specular Point Determination in the ECEF System

For GNSS-R, the glistening zone is always surrounding the SP. Therefore, the position of glistening zone could be obtained by determining the SP. The location of SP can be obtained with the steps shown in Fig. 4. More specific steps of this algorithm are discussed below.

In this process, all the coordinates are denoted in the ECEF system. $\vec{S} = [X_S, Y_S, Z_S]$ denotes the vector from the center of the earth to the SP. In order to get the SP, the initial guess of its location is assumed to be on the earth's surface immediately below the receiver, i.e., point V in Fig. 1(b). With this first-guessed specular vector $\vec{S}_{old}$, a iterative updating process is implemented. This process employs a modification vector $\vec{d}_S$ (Eq. (2)) to update $\vec{S}_{old}$. The modification vector $\vec{d}_S$ is the summation of two normalized vectors given by the following formula [2]:

$$\vec{d}_S = \frac{\vec{T} - \vec{S}_{old}}{\left| \vec{T} - \vec{S}_{old} \right|} + \frac{\vec{R} - \vec{S}_{old}}{\left| \vec{R} - \vec{S}_{old} \right|} \tag{2}$$

where $\vec{T}$, $\vec{R}$ and $\vec{S}_{old}$ represent the vectors from the centre of the earth

to the transmitter, receiver and SP in the ECEF coordinate system. $\vec{T} - \vec{S}_{old}$ indicates the incoming vector from the transmitter to the temporary SP, and $\vec{R} - \vec{S}_{old}$ indicates the reflected vector from the temporary SP to the receiver.

An intermediate vector is obtained as $\vec{S_{temp}} = \vec{S}_{old} + \vec{d_S}$. To ensure the new SP location is on the earth's surface after updating, the corrected SP vector must be scaled by the radius of the earth, r. Therefore, the new SP can be obtained using $\vec{S}_{new} = r\hat{S_{temp}}$ where $\hat{S_{temp}}$ is the unit vector of $\vec{S_{temp}}$.

Finally the modification vector $\vec{d_S}$ will be less than a threshold t_s which is pre-defined according to the demand of the location accuracy of SP. When $\vec{d_S} < t_s$, the position of SP is considered found. This position is the center of the glistening zone.

3.2. Coordinates Transformation from ECEF to ECXI System

This section defines a new Cartesian coordinate system which will be able to reinterpret the coordinates of the transmitter and receiver, and it will facilitate the calculation process of grid element coordinates. This system has its origin at the center of the earth. The SP is along the z-axis, xy plane is parallel to the plane tangent to the surface at the SP, and the x and z axes are in the incidence plane which is shown in Fig. 5. In the following paragraphs this coordinate system is referred
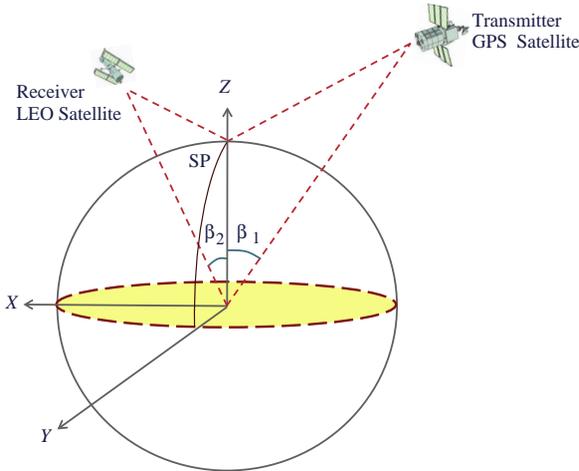

Figure 5. Earth-centered, X-Z incidence coordinate system.

to as the Earth-Centered, X-Z Incidence (ECXI) system.

In order to determine the ECXI coordinates of grid elements, two steps are required: 1) transform the locations and velocities of the transmitter and receiver from the ECEF coordinate system to the ECXI system; 2) conduct a coordinates calculating process for grid elements.

3.2.1. Transmitter and Receiver in the ECXI System

In order to facilitate the process of determining the coordinates of the grid elements of the ocean surface, both the locations and velocities of the transmitter and receiver need to be transformed to the ECXI system.

To represent the velocities of transmitter and receiver in the ECXI system, intermediate velocities in a East, North, Up (ENU) system [10] centred at the SP are calculated first. The conversion of velocity from the ECEF to the ENU coordinate system is given as

$$\begin{bmatrix} V_{x,enu} \\ V_{y,enu} \\ V_{z,enu} \end{bmatrix} = \begin{bmatrix} -\sin\lambda_s & \cos\lambda_s & 0 \\ -\sin\varphi_s\cos\lambda_s & -\sin\varphi_s\sin\lambda_s & \cos\varphi_s \\ \cos\varphi_s\cos\lambda_s & \cos\varphi_s\sin\lambda_s & \sin\varphi_s \end{bmatrix} \begin{bmatrix} V_{x_{ecef}} \\ V_{y_{ecef}} \\ V_{z_{ecef}} \end{bmatrix} \quad (3)$$

where λ_s and φ_s are the longitude and latitude of the SP, respectively. By applying the ECEF velocities in Eq. (3), the transmitter's ENU velocity $\vec{V}_{R_{enu}}$ and receiver's ENU velocity $\vec{V}_{T_{enu}}$ will be obtained. Converting the velocities into the ECXI system requires the horizontal components of the velocities $\vec{V}_{R_h} = [V_{R_{x,enu}}, V_{R_{y,enu}}]$ and $\vec{V}_{T_h} = [V_{T_{x,enu}}, V_{T_{y,enu}}]$.

Next, the angles between the y axis and the velocity vectors $\vec{V}_{R_h}$ and $\vec{V}_{T_h}$ are found as $\theta_{V_R} = \tan^{-1}(V_{R_{x,enu}}/V_{R_{y,enu}})$ and $\theta_{V_T} = \tan^{-1}(V_{T_{x,enu}}/V_{T_{y,enu}})$, respectively. A similar method may be used to determine the angle θ_r between the y axis and the horizontal component of the displacement vector from the receiver to the transmitter: $\vec{u}_h = [u_x, u_y]$, where $\vec{u} = \vec{T}_{enu} - \vec{R}_{enu}$. Then the angle between $\vec{u}_h$ and velocities $\vec{V}_{R_h}$ and $\vec{V}_{T_h}$ can be obtained by $\Delta\theta_R = \theta_{V_R} - \theta_r$, $\Delta\theta_T = \theta_{V_T} - \theta_r$. Finally, the velocities can be converted into the ECXI system:

$$\vec{V}_{R_n} = [|V_{R_h}|\cos(\Delta\theta_R), |V_{R_h}|\sin(\Delta\theta_R), V_{R_{z,enu}}] \quad (4)$$

$$\vec{V}_{T_n} = [|V_{T_h}|\cos(\Delta\theta_T), |V_{T_h}|\sin(\Delta\theta_T), V_{T_{z,enu}}]. \quad (5)$$

Converting the locations of transmitter and receiver to the ECXI system can be performed with the following steps: Given $\hat{R}$, $\hat{T}$ and $\hat{S}$ are the unit vectors from the earth center to the transmitter, receiver
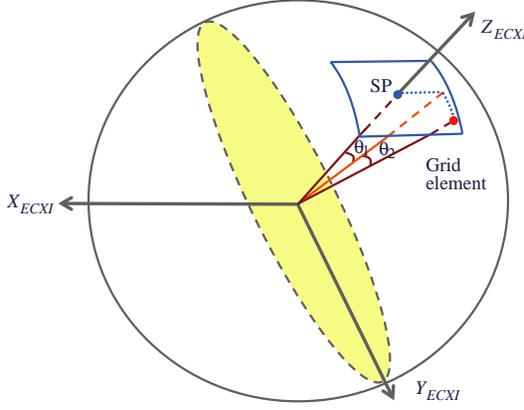
Figure 6. A grid element represented by the angles with respect to SP in x and y direction, respectively. The blue dot indicates the SP and the red dot indicates the gird element.

and SP, respectively, in the ECEF coordinate system, the angle β_1 and β_2 can be obtained by: $\beta_1 = \cos^{-1}(\hat{T} \cdot \hat{S})$ and $\beta_2 = \cos^{-1}(\hat{R} \cdot \hat{S})$. Then, in the ECXI system, $\vec{T}$ and $\vec{R}$ become

$$\vec{T}_n = [-|T|\sin(\beta_1), \ 0, \ |T|\cos(\beta_1)] \tag{6}$$

$$\vec{R}_n = [|R|\sin(\beta_2), \ 0, \ |R|\cos(\beta_2)]. \tag{7}$$

In the following paragraphs, all the vectors are designated in terms of the ECXI coordinate system.

3.2.2. Grid Elements in the ECXI System

The glistening zone is a spherical plane because of the curvature of the earth. Therefore, each grid element in ECXI system will be designated in terms of a pair of angles $(\theta_1, \ \theta_2)$ as shown in Fig. 6. When determining coordinates of the grid elements in the ECXI system, the bounds of these pairs are defined by the width and length of the glistening zone in relation to the distance from the earth center. For example, if the glistening zone is a circular area with radius r_g, then the bound of θ_1 and θ_2 would be $\phi_1 = \frac{r_g}{|\vec{S}_n|}$ and $\phi_2 = \frac{r_g}{|\vec{S}_n|}$, respectively, where $\vec{S}_n = (0, 0, r)$ is the position vector of SP in the ECXI system. In the process, the angle θ_1 ranges from $-\phi_1$ to ϕ_1 and the angle θ_2 ranges from $-\phi_2$ to ϕ_2. The position vector $\vec{\rho}(\theta_1, \theta_2)$ from the earth's center to grid element $(\theta_1, \ \theta_2)$ in the ECXI system can be obtained by

$\vec{\rho}(\theta_1, \theta_2) = \vec{S}_n M_1 M_2$ where the rotation matrix M_1 respect to θ_1 is [8]

$$M_1 = \begin{bmatrix} -\cos(\theta_1) & 0 & \sin(\theta_1) \\ 0 & 1 & 0 \\ \sin(\theta_1) & 0 & \cos(\theta_1) \end{bmatrix} \qquad (8)$$

and the rotation matrix M_2 respect to θ_2 is

$$M_2 = \begin{bmatrix} 1 & 0 & 0 \\ 0 & \cos(\theta_2) & -\sin(\theta_2) \\ 0 & \sin(\theta_2) & \cos(\theta_2) \end{bmatrix} \qquad (9)$$

For simplicity, $\vec{\rho}(\theta_1, \theta_2)$ is referred hereafter as $\vec{\rho}$.

3.3. Power Distribution in Spatial and DD Domain

This process includes the following steps: determine the Doppler shift, C/A delay and scattering coefficient of each grid element, and map the power distribution received by a GNSS-R receiver from the spatial domain into the DD domain.

3.3.1. Doppler Frequency Shift

The Doppler frequency shift f_d is caused by the relative motion between the transmitter, receiver and grid elements. It can be obtained using [2]

$$f_d(\vec{\rho}) = \frac{\left[\left(\vec{V}_S - \vec{V}_T \right) \cdot \hat{m} \right] f_l}{c} + \frac{\left[\left(\vec{V}_R - \vec{V}_S \right) \cdot \hat{n} \right] f_l}{c} + f_{clk} \qquad (10)$$

where $\vec{V}_T$, $\vec{V}_R$ and $\vec{V}_S$ represent the velocity of transmitter, receiver and a grid element, respectively. f_l is the L_1 carrier frequency $= 1575.42\,\text{MHz}$. $\hat{n}$ is the unit vector of the scattered wave and $\hat{m}$ is the unit vector of the incident wave [8]. f_{clk} denotes the Doppler shift caused by the receiver clock drift assumed here to be 0. In [11], it shows that time-evolving or dynamic ocean surface (grid element) will produce a non-zero Doppler shift. With consideration of the non-zero grid element speed, it might be helpful to retrieve the sea surface parameters such as wind and wave information from the GNSS-R DDM. Here, the velocity of sea surface $\vec{V}_s$ has been assumed as zero since the magnitude of grid element velocity is much smaller than the speed of transmitter and receiver [2, 9]. The main purpose in this paper is to investigate the oil slick effect on the GNSS DDM, the influence of non-zero grid element speed is ignored for simplicity. For SP, the frequency shift is $f_d = \frac{f_l}{c}(-\vec{V}_{Tn} \cdot \frac{\vec{S}_n - \vec{T}_n}{|\vec{S}_n - \vec{T}_n|} + \vec{V}_{Rn} \cdot \frac{\vec{R}_n - \vec{S}_n}{|\vec{R}_n - \vec{S}_n|})$, and then Δf in the variables explanation of Eq. (1) can be acquired using $f_d(\vec{\rho})$ and f_d.

3.3.2. C/A Delay

C/A delay refers to the time delays of signals reflected from different grid elements which is given by $\tau(\vec{\rho}) = \frac{f(R_\rho + T_\rho)}{c}$ where R_ρ and T_ρ are the distances from the grid element to the receiver and transmitter, respectively; $f = 1.023 \times 10^6$ Hz is the frequency of C/A code. For SP, the C/A delay is $\tau = \frac{f}{c}(|\vec{R}_n - \vec{S}_n| + |\vec{T}_n - \vec{S}_n|)$, and then $\Delta\tau$ in the variables explanation of Eq. (1) can be acquired using $\tau(\vec{\rho})$ and τ.

With the knowledge of both the DD coordinate and spatial coordinate of each grid element, the relationship between the DD and spatial domain is obtained.

3.3.3. Scattering Coefficient Distribution

The power received from each grid element is closely related to the scattering coefficient distribution of it. The equation to determine scattering coefficient is [9]

$$\sigma^0 = \pi |\Re|^2 \left(\frac{|\vec{q}|}{q_z} \right)^4 P \left(-\frac{\vec{q}_\perp}{q_z} \right) \tag{11}$$

where $|\Re|^2$ is the Fresnel reflection coefficient. It is determined by the polarization, the complex dielectric constant of sea water, and the local elevation angle [9]. The scattering vector is defined as $\vec{q} \equiv k(\hat{n} - \hat{m}) \equiv \vec{q}_\perp + q_z \hat{z}$ where k is the carrier wave number. It can be obtained with the locations of the transmitter, receiver and corresponding grid element. $P(-\frac{\vec{q}_\perp}{q_z})$ is the probability density function (PDF) of the given ocean surface slope. For arbitrary wind direction, the PDF is provided in [8]. Here, for simplicity, the wind direction is assumed to be along x axis of the ECXI system, then the PDF can be approximated by [9]

$$P \left(-\frac{\vec{q}_\perp}{q_z} \right) = \frac{1}{2\pi\sigma_u\sigma_c} \exp \left[-\frac{1}{2} \left(\frac{\left(-\frac{q_{\perp,u}}{q_z} \right)^2}{\sigma_u^2} + \frac{\left(-\frac{q_{\perp,c}}{q_z} \right)^2}{\sigma_c^2} \right) \right] \tag{12}$$

where $-\frac{q_{\perp,u}}{q_z}$, $-\frac{q_{\perp,c}}{q_z}$ represents the upwind and crosswind ocean slope components, respectively; and σ_u^2, σ_c^2 indicates the upwind and crosswind Mean-Square Slope (MSS) component, respectively, which is given by Cox and Munk in [12]

$$\begin{aligned} \sigma_{c,c}^2 &= 0.003 + 1.92 \times 10^{-3} U_{10} \\ \sigma_{u,c}^2 &= 3.16 \times 10^{-3} U_{10} \end{aligned} \tag{13}$$

$$\sigma_{c,s}^2 = 0.003 + 0.84 \times 10^{-3} U_{10}$$
$$\sigma_{u,s}^2 = 0.005 + 0.78 \times 10^{-3} U_{10} \tag{14}$$

In which, the second subscript of MSS c stands for "clean" and s stands for "slick". U_{10} is the wind speed (WS) at $10\,\mathrm{m}$ height from the surface. Since this model is originally raised for optical wavelengths signals, in order to apply the model to L band GNSS-R signals, the empirical modification in [13] is adopted in the simulation. The MSS of certain area is determined by the WS and the presence of oil spill. Hence, oil slicks on the ocean surface will affect the scattering coefficient distribution and thus change the corresponding DDM.

3.3.4. Mapping Received Power to DD Domain

Before calculating received power, the Σ of each grid element in spatial domain can be obtained using

$$\Sigma(\vec{\rho}) = \frac{T_i^2 D^2(\vec{\rho}) \sigma^0(\vec{\rho}) ds}{4\pi R_R^2(\vec{\rho}) R_T^2(\vec{\rho})} \tag{15}$$

where ds is the area of each grid element. Using the relationship between the spatial domain and DD domain, the Σ function can be mapped into the DD domain. Hence, $\Sigma(\Delta f, \Delta \tau)$ would be acquired.

The expression of DDM in Eq. (1) can be rewritten as [14]

$$\langle |Y(\Delta\tau, \Delta f)|^2 \rangle = \chi^2(\Delta\tau, \Delta f) * \Sigma(\Delta\tau, \Delta f) \tag{16}$$

where "$*$" indicates two dimensional convolution and $\chi(\Delta\tau, \Delta f) \approx \Lambda(\Delta\tau) S(\Delta f)$ is the Woodward ambiguity function (WAF) [9]. By taking advantage of the properties of the Fourier transformation ($\mathscr{F}[\cdot]$), Eq. (16) becomes [15]:

$$\mathscr{F}[\langle |Y(\Delta\tau, \Delta f)|^2 \rangle] = \mathscr{F}[\Sigma(\Delta\tau, \Delta f)] \cdot \mathscr{F}[\chi^2(\Delta\tau, \Delta f)]. \tag{17}$$

Therefore, rather than conducting the convolution of WAF and Σ, multiplication of the Fourier transformations could be used to save time [14]. Then, by conducting the inverse Fourier transformation, DDM $\langle |Y(\Delta\tau, \Delta f)|^2 \rangle$ will be acquired.

4. RESULTS

The scattering coefficient distribution is modelled by the oil spill occurred in Gulf of Mexico in 2010. The image used to model the slick-covered area is acquired by the Moderate Resolution Imaging Spectroradiometer (MODIS) launched by NASA. A uniformly distributed $6.8\,\mathrm{m/s}$ WS at daytime is taken into account according

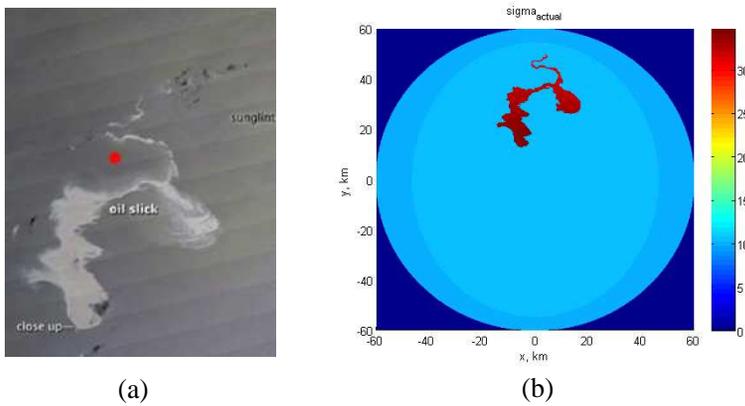(a)   (b)

Figure 7. (a) Photo of the oil spill at gulf of Mexico, April 25, 2010. The red spot indicates the location of Station 42040. (b) Simulated scattering coefficient distribution.
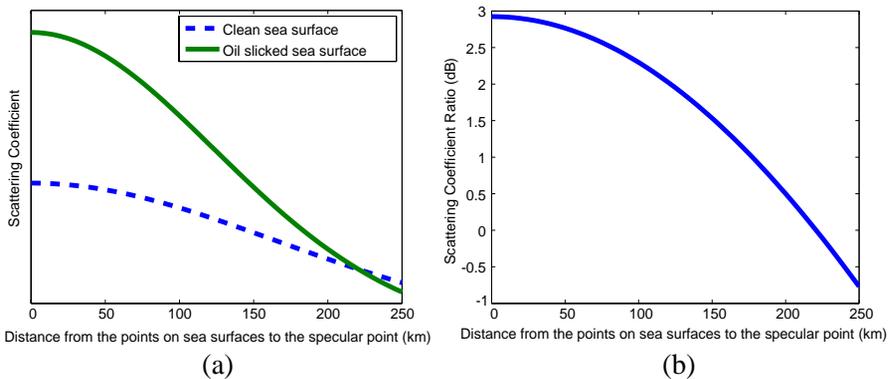

(a)   (b)

Figure 8. (a) Scattering coefficients of oil contaminated areas and clean areas versus distance to the specular point. (b) The ratio between the scattering coefficients of oil slick and clean sea surfaces.

to data from Station 42040 of National Data Buoy Center [16] as shown in Fig. 7(a). In the simulation result of σ^0 in Fig. 7(b), the oil slicked area can be clearly distinguished. It should be noted that the scattering coefficient of the oil slick, compared with that of the clean ocean surfaces, decreases more rapidly when the scattering point moves away from the SP, because the diffuse reflection becomes stronger and occurs more frequently on clean surfaces than oil contaminated areas. Although the glistening zone could be more
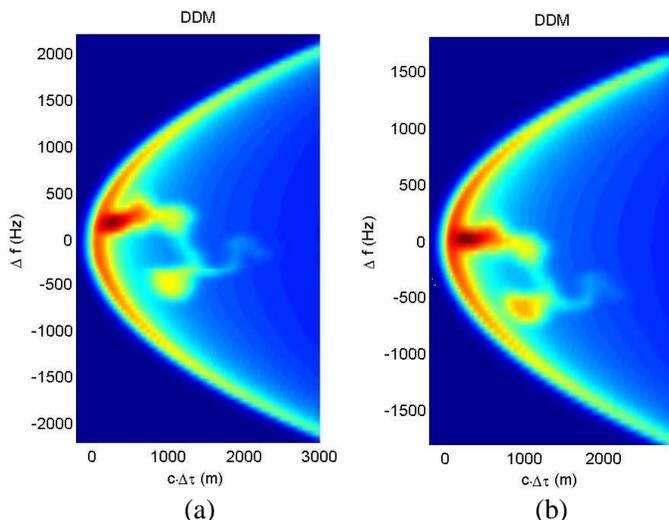
Figure 9. Simulated DDM. (a) Simplified scenario. (b) General scenario.

than 400 km in diameter [14], the area of oil slick detection should be determined by the region where the scattering coefficients of oil slick are distinguishable. Fig. 8(a) shows the scattering coefficients of both oil slicked areas and clean ocean surfaces at the WS of 6.8 m/s, and Fig. 8(b) shows the ratio of the scattering coefficients of the two. As can be observed in these figures, the scattering coefficients of the two types of surfaces becomes identical at scattering points 220 km away from the SP, which suggests that the oil slick could be detected within this range limit. However, in order to achieve a large contrast between oil contaminated and clean surfaces so that the detection result will not be severely affected by noise, the radius of the detection area would have to be further reduced (120 km for 2 dB contrast and 80 km for 2.5 dB contrast, according to Fig. 8(b)).

Both a simplified scenario and a general scenario are employed to generate DDMs based on Fig. 7(b). The simplified scenario is similar to the one applied by Valencia in [7], and the general scenario is the same with the simplified scenario except for the location and velocity of the receiver. A more specific description of the scenarios is shown in Table 1. The corresponding simulation results is shown in Fig. 9. As can be observed from the result, the simulated DDMs of the two scenarios are different especially in the oil slicked area. The shape of the oil spill in the general scenario is slightly "twisted", because the

Table 1. General and simplified scenarios.

	General Scenario	Simplified Scenario
Transmitter Position (10^6 m)	0, 0, 26682	0, 0, 26682
Transmitter Velocity (m/s)	0, −3000, 0	0, −3000, 0
Receiver Position (10^6 m)	1286, 1345, 6800	0, 0, 7050
Receiver Velocity (m/s)	4000, 3000, 0	0, 5000, 0
Elevation angle at SP	72.3°	90° (nadir reflection)
Coherent integration times	10 ms	10 ms

variation in the orbiting direction of the transmitter and receiver may alter the contours of the iso-Doppler-frequency, so that the oil spill distribution in the DD domain is rearranged.

As mentioned before, the application of the general scenario is broader than that of the simplified scenario, through which the passive GNSS-R receiver is more likely to detect the oil slick on the sea surface. Moreover, for a GNSS-R system with the antenna beam steered away from nadir by a small angle, e.g., the one used on the UK-DMC satellite [17], the DDM with the highest SNR could be obtained only under the general scenario, with the elevation angle set accordingly to the antenna steering angle.

5. CONCLUSION

This paper discusses the DDM simulation process on an oil slicked area under a general scenario. Specifically, the details on how to extend the simulating process from a simplified scenario to a general scenario is discussed. An analysis of the received power from oil contaminated and clean sea surface indicates the radius of the oil slick detection area is about 100 km. In the simulation result, the difference between the two scenarios due to the general scenario can be observed clearly. Thus, applying the GNSS-R DDM of oil slicks under general scenarios could enhance the study of oil spill detection. Further work is required to conduct the scattering coefficient retrieval from the generated DDMs in order to detect the oil slick.

his editorial help of this paper. The authors would also like to thank C. X. Shen for his revision.

REFERENCES

1. Martin-Neira, M., "A passive reflectometry and interferometry system (PARIS): Application to ocean altimetry," *ESA J.*, Vol. 17, 331–355, 1993.

2. Gleason, S., "Towards sea ice remote sensing with space detected GPS signals: Demonstration of technical feasibility and initial consistency check using low resolution sea ice information," *Remote Sens.*, Vol. 2, 2017–2039, 2011.

3. Gleason, S., S. Hodgart, Y. Sun, C. Gommenginger, S. Mackin, M. Adjrad, and M. Unwin, "Detection and processing of bistatically reflected GPS signals from low earth orbit for the purpose of ocean remote sensing," *IEEE Trans. Geosci. Remote Sens.*, Vol. 43, No. 6, 1229–1241, 2005.

4. Jin, S., G. Feng, and S. Gleason, "Remote sensing using GNSS signals: Current status and future directions," *Adv. Space Res.*, Vol. 47, No. 10, 1645–1653, 2011.

5. Wiehl, M., B. Legresy, and R. Dietrich, "Potential of reflected GNSS signals for ice sheet remote sensing," *Progress In Electromagnetics Research*, Vol. 40, 177–205, 2003.

6. Pinel, N., C. Bourlier, and J. Saillard, "Forward radar propagation over oil slicks on sea surfaces using the Ament model with shadowing effect," *Progress In Electromagnetics Research*, Vol. 76, 95–126, 2007.

7. Valencia, E., A. Camps, H. Park, and N. Rodriguez-Alvarez, "Oil slicks detection using GNSS-R," *IGARSS*, 4383–4386, Vancouver, BC, Canada, 2011.

8. Gleason, S. and D. Gebre-Egziabher, *GNSS Applications and Methods*, Artech House, Norwood, 2009.

9. Zavorotny, V. U. and A. G. Voronovich, "Scattering of GPS signals from the ocean with wind remote sensing application," *IEEE Trans. Geosci. Remote Sens.*, Vol. 38, No. 2, 951–964, 2000.

10. "Wikipedia, geodetic system," Sep. 13, 2012, Internet: http://en.wikipedia.org/wiki/Geodetic_system.

11. Hayslip, A. R., J. T. Johnson, and G. R. Baker, "Further numerical studies of backscattering from time-evolving nonlinear sea surfaces," *IEEE Trans. Geosci. Remote Sens.*, Vol. 41, No. 10, 2287–2293, 2003.

12. Cox, C. and W. Munk, "Measurement of the roughness of the sea surface from photographs of the sun's glitter," *J. Opt. Soc. Am.*, Vol. 44, No. 11, 838–850, 1954.

13. Katzberg, S. J., O. Torres, and G. Ganoe, "Calibration of reflected GPS for tropical storm wind speed retrievals," *Geophys. Res. Lett.*, Vol. 33, 18602, 2006.

14. Marchan-Hernandez, J., A. Camps, N. Rodriguez-Alvarez, E. Valencia, X. Bosch-Lluis, and I. Ramos-Perez, "An efficient algorithm to the simulation of delay-Doppler maps of reflected global navigation satellite system signals," *IEEE Trans. Geosci. Remote Sens.*, Vol. 47, No. 8, 2733–2740, 2009.

15. Valencia, E., A. Camps, J. F. Marchan-Hernandez, H. Park, X. Bosch-Lluis, N. Rodriguez-Alvarez, and I. Ramos-Perez, "Ocean surface's scattering coefficient retrieval by delay-Doppler map inversion," *IEEE Geosci. Remote Sens. Lett.*, Vol. 8, No. 4, 750–754, 2011.

16. "National data buoy center," Sep. 2, 2012, Internet: http://www.ndbc.noaa.gov/station_history.php?station=42040.

17. Gleason, S., "Remote sensing of ocean, ice and land surfaces using bistatically scattered GNSS signals from low earth orbit," Ph.D. Thesis, Univ. Surrey, Guildford, 2006.